The samples resulted from constructive interactions with Mr. M. Schneider, E. Bucker, and Dr. R. W. Francis. We wish to express our thanks to Dr. J. A. Amick for his encouragement during the course of this work.

Manuscript received March 7, 1983.

Any discussion of this paper will appear in a Discussion Section to be published in the June 1984 JOURNAL. All discussions for the June 1984 Discussion Section should be submitted by Feb. 1, 1984.

Exxon Research and Engineering Company assisted in meeting the publication costs of this article.

REFERENCES

1. M. V. Sullivan and J. H. Eigler, *This Journal*, **104**, 226 (1956); H. Iwasa, M. Yokozawa, and I. Teramoto, *ibid.*, **115**, 485 (1968).
2. G. Gutzeit, *Plating*, **46**, 1158, 1275, 1377 (1959); **49**, 63 (1960).
3. J. P. McCloskey, *ibid.*, **51**, 689 (1964).
4. Reviewed in K. M. Gorbunova, A. A. Nikiforova, and G. A. Sadakov, "Achievements of Science: Chemistry, Electrochemistry, 1965," S. S. Kruglikov, Editor (1965).
5. M. M. Critchfield, C. H. Dungan, J. H. Letchev, V. Mark, and J. R. Von Water, "^{31}P Nuclear Magnetic Resonance," John Wiley and Sons, New York (1967).
6. M. M. Critchfield, C. H. Dungan, J. H. Letchev, V. Mark, and J. R. Von Water, "^{31}P Nuclear Magnetic Resonance," pp. 289-290, John Wiley and Sons, New York (1967).

Semiconductor Electrodes

XLIX. Evidence for Fermi Level Pinning and Surface-State Distributions from Impedance Measurements in Acetonitrile Solutions with Various Redox Couples

G. Nagasubramanian, B. L. Wheeler, and A. J. Bard*

Department of Chemistry, University of Texas, Austin, Texas 78712

ABSTRACT

Capacitance-voltage (C-V) measurements were made for the single crystal semiconductors n-TiO_2, n-CdS, n-InP, p-Si, p-GaAs, n- and p-WSe_2, and n-$MoSe_2$ in acetonitrile containing a number of redox couples whose potentials (V_{redox}) spanned a potential regime much wider than the bandgaps. The flatband potential (V_{FB}) evaluated from capacitance-potential (*C-V*) measurements (Mott-Schottky plots) exhibited three types of behavior with varying solution redox potentials: (*i*) V_{FB} varied monotonically with V_{redox} for p-Si, p-GaAs, and n-InP; (*ii*) for n-TiO_2 and n-CdS, V_{FB} did not shift for couples located negative of the midgap potential, but varied monotonically for couples positive of this value; (*iii*) for the layer-type, compounds ($MoSe_2$, WSe_2), V_{FB} was almost independent of V_{redox}. These differences were ascribed to differences in surface-state densities. For n-TiO_2 crystals, (001) face etched with molten $KHSO_4$ and reduced, evidence for surface states at two different potentials was obtained from the in-phase component of the total admittance. Tentative assignment of these states is to lattice defects. The states closer to the conduction band are assigned to oxygen vacancies and the deeper states to Ti (III). The densities of surface states (N_{ss}) evaluated from G_p/ω *vs.* ω plots for TiO_2 and p-Si are around 10^{10} and 10^{13} cm^{-2}, respectively. These two values represent different situations, *i.e.*, while the former value of N_{ss} is not sufficient for pinning the Fermi level, the latter value is sufficiently high for the occurrence of Fermi level pinning.

There has been increasing evidence, based on measurements of open-circuit photopotentials (V_{oc}) developed by semiconductor electrodes, that the model for the semiconductor/liquid interface (1), in which the bandedges remain fixed in the presence of different redox couples, often does not hold. The observed effect is that V_{oc} is relatively independent of V_{redox}, the potential of the redox couple in solution. This has been ascribed to Fermi level pinning (FLP) (2) in the presence of a high density of interface or surface states. Under these conditions, a change in potential across the semiconductor/solution interface is largely absorbed by a change in the potential drop across the Helmholtz layer rather than across the space charge layer within the semiconductor (Fig. 1). Thus, in the presence of FLP, the flatband potential, V_{FB}, changes with V_{redox} so that $V_{oc} \approx |V_{FB} - V_{redox}|$ remains relatively constant. This shift of V_{FB} with V_{redox} has not been the subject of many investigations. Previously, we have shown by capacitance measurements that V_{FB} shifts for p-Si in MeCN solutions (3). In this paper, we extend these studies to several other semiconductor materials. We might note that FLP is also well known for semiconductor/metal junctions where the barrier height across the junction for a given semiconductor, *e.g.*, GaAs, is found to be independent of the metal work functions (4).

Even with large bandgap materials, surface states may mediate interfacial electron transfer processes in PEC cells (5-10). Surface states can also affect the efficiency of PEC cells, *e.g.*, by acting as recombination centers or by abetting dark backreactions. For example, the shape of the photocurrent *vs.* applied bias curve can be used as a measure of efficiency of a PEC cell; the precipitous increase in photocurrent near V_{FB} for n-TiO_2 etched in a special way with simmering H_2SO_4 was taken as a sign of improvement (11). Such a sharp rise to the saturation value has been attributed to an absence of recombination sites and surface states (12). The dependency of the Schottky barrier heights on metal work function with large bandgap materials, such as TiO_2 and $SrTiO_3$ solid-state devices

* Electrochemical Society Active Member.
Key words: capacitance, flatband potential, conductance.

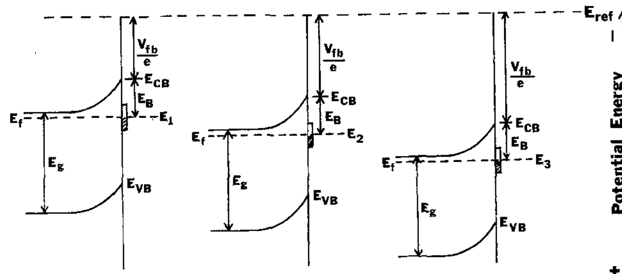

Fig. 1. Scheme 1. Position of bandedges upon variation of the redox energy level of the contacting medium (E_1, E_2, E_3) for a Fermi level pinned n-type semiconductor. E_B is invariant with E_i, while V_{FB} varies with respect to the energy level of a reference electrode, E_{ref}.

Downloaded 12 Feb 2009 to 146.6.143.190. Redistribution subject to ECS license or copyright; see http://www.ecsdl.org/terms_use.jsp

(13), has been attributed to the absence of a high density of surface states. Further, the absence of surface states is sometimes assumed when frequency independent Schottky-Mott (S-M) plots (plots of C^{-2} *vs.* V, where C is capacitance) are found. However, we (14) and others (15-17) have shown that with small bandgap semiconductors, the in-phase (0°, conductance) component of the total admittance is more sensitive to the presence of surface states than the quadrature (90°, capacitance) component (see Appendix).

We report here a-c impedance studies of several single-crystal semiconductors in MeCN and show that V_{FB} shifts with V_{redox} occur with several of these. The effect of pretreatment of TiO_2 on its impedance behavior and investigation of surface states by conductance measurements are also discussed.

Experimental

The single crystals employed were n-TiO_2, n-InP, n-CdS, n- and p-WSe_2, n-$MoSe_2$, p-Si, and p-GaAs. The procedures for polishing and mounting the semiconductor electrodes have been described elsewhere (18-24) and the etching procedures are given in Table I. Two different types of TiO_2 crystals were employed. The undoped TiO_2 single crystal (Nakazumi Earth Crystals, Japan) is denoted crystal A and the Nb-doped TiO_2 crystal, obtained from H. S. Jarrett, du Pont, is denoted crystal B. Both were oriented with the (001) face exposed to solution, as ascertained by x-ray diffraction (ASTM Card No. 23-1486). Some crystals were treated by a procedure recommended by Jarrett to produce a smooth surface (treatment 1). These were polished in succession with 0.3 μm alumina and 1 μm diamond paste to produce a mirror-like surface. This surface was then etched with molten $KHSO_4$ in a Pt crucible (625°C) for 2 hr. An SEM photograph (Fig. 2) shows a very smooth surface. Since the crystals had a straw-colored appearance after the molten $KHSO_4$ etch, implying that they were oxidized, they were subjected to a reduction pretreatment before use. The Nb-doped crystals were reduced in flowing CO at 700°C for 1 hr, the undoped crystals were reduced in an H_2 atmosphere at 625°C for 20 min. These were mounted as electrodes and used without further treatment. In treatment 2, the undoped TiO_2 crystals were not etched with $KHSO_4$, but instead were only reduced in H_2 (625°C for 20 min) directly after polishing with Al_2O_3 and diamond paste. The methods of purification of the solvent acetonitrile (MeCN) and sources of redox couples are given elsewhere (18). Abbreviations of the various redox couples employed are given in Table II. Their concentrations varied from 0.1 to 30 mM. With perylene, rubrene, chrysene, and $MV(PF_6)_2$ (where MV = methyl viologen) the concentrations were about 0.1 m*M*; for $Ru(bpy)_3^{2+/+}$, and $AQ^{0/-}$ (where bpy = bipyridine and AQ = anthraquinone) they were about 0.5 and 2 m*M*, respec-

Table I. Doping density and etching procedures for different semiconductors

SC	$N_{D(A)}/cm^3$	Etching procedures
TiO_2	~10^{19}	Conc HNO_3 for 1 min followed by conc HF for 10 sec, then rinsed with distilled water. This procedure was repeated twice.
CdS	~10^{17}	Conc HCl for 40 sec, then rinsed with distilled water.
n-WSe_2, n-$MoSe_2$, p-WSe_2	~10^{15}	6*M* HCl for 30 sec, then rinsed with distilled water. This procedure was repeated twice.
n-InP	~10^{16}	6*M* HCl for 30 sec, then rinsed with distilled water.
p-GaAs	~10^{15}	H_2SO_4:H_2O_2(30%):H_2O (3:1:1 by volume) solution for 5 sec, then rinsed with distilled water.
p-Si	~10^{15}	HNO_3:CH_3COOH:HF, (3:1:3 by volume) containing a drop of Br_2 per 50 ml for 30 sec followed by conc HF for 5 sec, then rinsed with distilled water.

Table II. V_{FB} of various semiconductors in MeCN containing different redox couples. The values in the parentheses represent V_{redox} vs. SCE

SC	Blank	1 $CHR^{0/+}$ (1.56)	2 $Th^{0/+}$ (1.26)	3 $Per^{0/+}$ (1.14)	4 $Rub^{0/+}$ (0.94)	5 $10\text{-}MP^{0/+}$ (0.79)	6 $Fe(Cp)_2^{0/+}$ (0.53)	7 $TMPD^{0/+}$ (0.27)	8 $Fe(\eta^5\text{-}C_5Me_5)_2$ (−0.12)	9 $OX^{0/+}$ (−0.2)	10 $MV^{2+/+}$ (−0.43)	11 $BQ^{0/-}$ (−0.56)	12 $AQ^{0/-}$ (−0.96)	13 $Ru(bpy)_3^{2+/+}$ (−1.27)	14 $PhNO_2^{0/-}$ (−1.33)	15 $Ph(CN)_2^{0/-}$ (−1.72)
TiO_2	~−1.0	−0.13		−0.18	−0.42	−0.7	−0.82	−1.0	−1.0							
n-CdS	−0.9		−0.2			−0.4	−0.7	−0.8								
n-WSe_2	−0.3		−0.4			−0.4		−0.4								
n-$MoSe_2$	+0.1		−0.1			0.0		−0.12								
p-WSe_2	0.78										0.75	0.62		0.8	0.75	
n-InP	−0.75	−0.2	0.05				−0.31				−0.5					
p-GaAs	0.06											−0.06	−0.14		−0.33	−0.46
p-Si	+0.15									−0.02		−0.12	−0.44	−0.52	−0.53	

1, CHR = Chrysene; 2, Th = Thianthrene; 3, Per = Perylene; 4, Rub = Rubrene; 5, 10-MP = 10-Methylphenothiazine; 6, $Fe(Cp)_2$ = Ferrocene; 7, TMPD = N, N, N′, N′-Tetramethyl-*p*-phenylenediamine; 8, $Fe(\eta^5\text{-}C_5Me_5)_2$ = Decamethyl Ferrocene; 9 OX-1 = Oxazine-1; 10, MV = Methyl Viologen; 11, BQ = *p*-Benzoquinone; 12, AQ = 9,10-Anthraquinone; 13, $Ru(bpy)_3$ = Ruthenium (tris-bipyridine); 14, $PhNO_2$ = Nitrobenzene; 15, $Ph(CN)_2$ = Phthalonitrile.

Downloaded 12 Feb 2009 to 146.6.143.190. Redistribution subject to ECS license or copyright; see http://www.ecsdl.org/terms_use.jsp

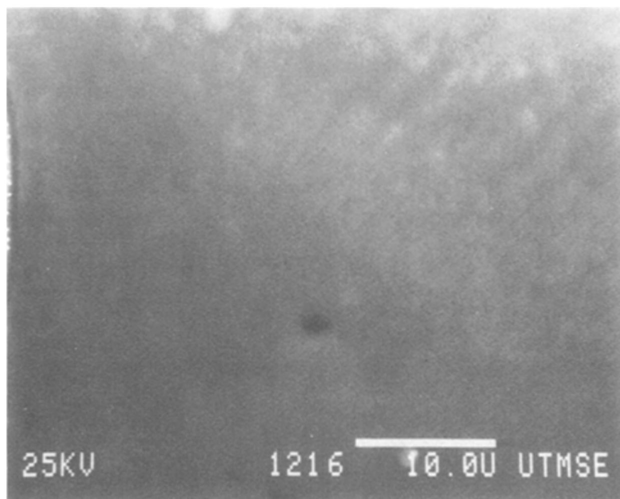

Fig. 2. Scanning electron micrograph of TiO_2 after etching with $KHSO_4$ for 2 hr in Pt crucible.

tively. Nitrobenzene used with p-Si was about 30 m*M*. All other couples were 10 m*M*. The concentrations of the electrochemically generated forms were about 20-30% of the starting material. The supporting electrolyte was electrometric grade tetra-n-butylammonium perchlorate (TBAP) (Southwestern Analytical Chemicals, Austin, Texas). This was purified by dissolving it in a minimum quantity of acetone, filtering the solution, and then recrystallizing with ether. This procedure was repeated twice. The recrystallized TBAP was dried for two days at 80°C under vacuum ($<10^{-5}$ Torr). All chemicals were stored in a helium-filled glove box (Vacuum Atmosphere Corporation, Hawthorne, California).

A conventional two-compartment electrochemical cell of ~25 ml capacity was used for electrochemical studies. For impedance measurements, a large area (~40 cm^2) Pt-gauze immersed in the same compartment as the working electrode was used as a counterelectrode. A Pt-gauze (~10 cm^2), separated from the main compartment by a medium porosity glass frit, was used as a counterelectrode for electrochemically generating radicals. An aqueous SCE with a KCl-saturated agar plug, directly introduced into the main compartment, was used as the reference electrode. All the potentials are expressed against this aqueous SCE unless otherwise specified.

A PAR Model 173 potentiostat and a PAR 175 universal programmer (Princeton Applied Research Corporation, Princeton, New Jersey) equipped with a Model 2000 X-Y recorder (Houston Instruments, Austin, Texas) were used to obtain the cyclic voltammograms as well as for capacitance-voltage measurements. A Soltec (Sun Valley, California) Model 6432, X-Y_1Y_2 recorder was used for recording both the 0° and 90° components simultaneously. In these latter experiments, a lock-in amplifier technique, which yields the in-phase and the out-of-phase components of an a-c signal superimposed on a linear sweep, was used. The a-c signal (~12 mV peak-to-peak) at different frequencies was obtained for input into the potentiostat from a Model 200CD wide range oscillator (Hewlett-Packard, Palo Alto, California). Its components at 0° and 90° were obtained by using either a PAR Model HR-8 or a PAR Model 5204 lock-in amplifier. An MINC-11 (Digital Equipment Corporation, Marlboro, Massachusetts) computer could also be used for continuous data acquisition from the lock-in amplifier, and a Houston Instruments digital plotter (Model DMP-5) was used for the data output. The experimental apparatus and procedures are similar to those previously described (3) and will be described in more detail in a separate paper. All solutions were prepared and sealed inside the glove box prior to removal for experimentation.

Results

C-V data.—Capacitance values were obtained for a number of single-crystal semiconductors in 0.1*M* TBAP MeCN solutions as a function of frequency and applied potential in the absence and presence of various redox couples spanning a wide range of V_{redox}. The flatband potential *vs.* an aqueous SCE, V_{FB}, was then determined from a Schottky-Mott (S-M) plot of $1/C^2$ *vs.* V

$$\frac{1}{C^2} = \frac{2}{e\epsilon\epsilon_0 N}(V - V_{FB} - 0.025) \quad [1]$$

where C is the capacitance per unit area; e, the electronic charge (1.6×10^{-19} C); ϵ, the semiconductor dielectric constant; ϵ_0, the permittivity of free space (8.85×10^{-14} F/cm); and N, the acceptor (p-type) or donor (n-type) density. Although in some cases determination of V_{FB} from the intercept of S-M plots involves some ambiguity (25), V_{FB} can generally be determined to within 0.1V, and shifts in V_{FB} can quite readily be determined from the C-V plots themselves. As shown previously (3), linear S-M plots which yield V_{FB} can be obtained in the presence of surface states when the frequency used to obtain the capacitance is such that the surface-state capacitance does not make an appreciable contribution. In Fig. 3 are given the S-M plots for unetched TiO_2 (crystal A, treatment 2) in supporting electrolyte alone at three different frequencies; in Fig. 4a, b, the C-V and the corresponding S-M plots, respectively, are shown for a solution containing the $TMPD^{0/+}$ couple (abbreviations used are given in Table II). Although the V_{FB} for n-TiO_2 in the absence and presence of the $TMPD^{0/+}$ couple is the same, addition of other redox couples, such as 10-$MP^{0/+}$ or $Per^{0/+}$, causes an appreciable shift of V_{FB} to more positive values. The results are summarized in Table II. Similar shifts in V_{FB} with V_{redox} are found with n-CdS and n-InP (Fig. 5 and 6). In Fig. 7, the plots of variation of V_{FB} with V_{redox} are given for p-Si, p-GaAs, p-WSe_2, and n-InP along with n-TiO_2 and n-CdS. Note however, that for the layer-type compounds n-WSe_2, n-$MoSe_2$, and p-WSe_2, V_{FB} is essentially invariant with V_{redox}. This finding agrees with a previous study of the C-V behavior of another layer-type compound, α-$MoTe_2$, where V_{FB} was independent of V_{redox} (14).

The behavior of the semiconductors which show shifts of V_{FB} with V_{redox} is consistent with FLP and the presence of surface states on the electrode surface. The density and distribution of these states can be

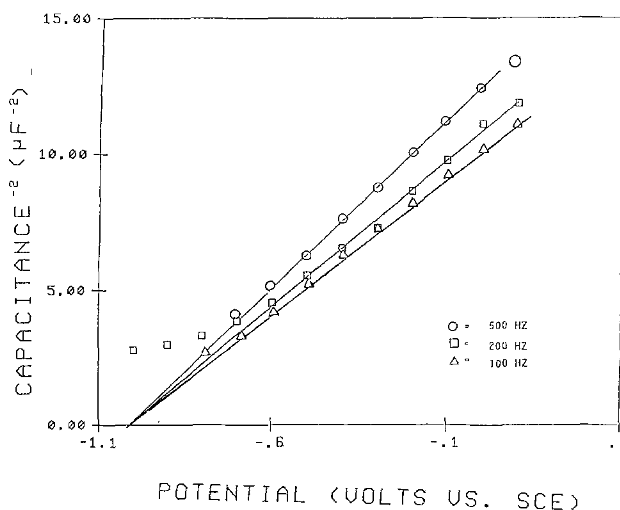

Fig. 3. Schottky-Mott (S-M) plots for TiO_2 contacting MeCN, containing 0.1*M* TBAP only.

Downloaded 12 Feb 2009 to 146.6.143.190. Redistribution subject to ECS license or copyright; see http://www.ecsdl.org/terms_use.jsp

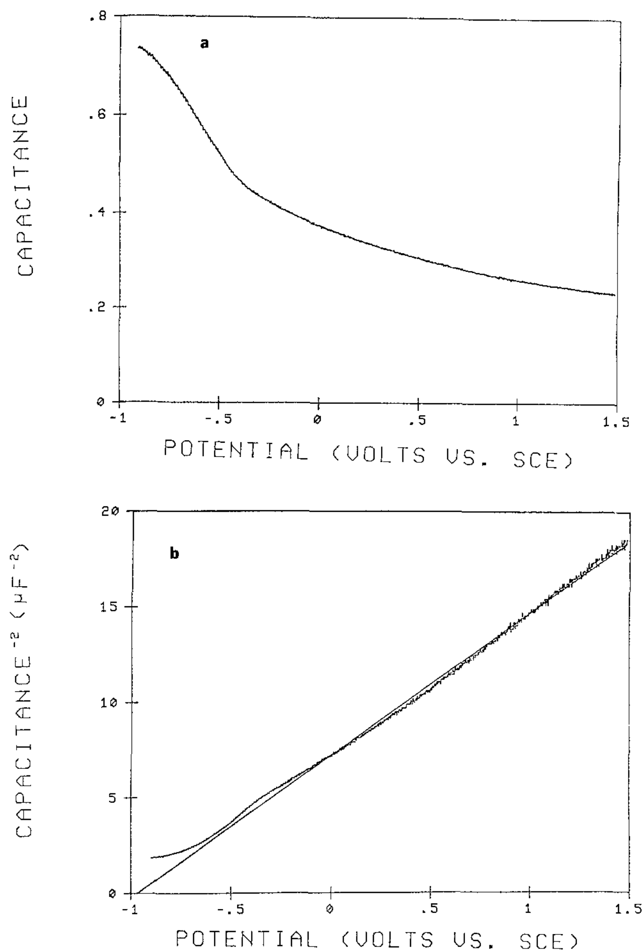

Fig. 4. (a) Capacitance (*C*) *vs.* potential of TiO_2/MeCN containing 10 m*M* TMPD and 2 m*M* $TMPD^+$ in 0.1*M* TBAP; *f* = 200 Hz; (b) S-M plot for the *C-V* curve in (a).

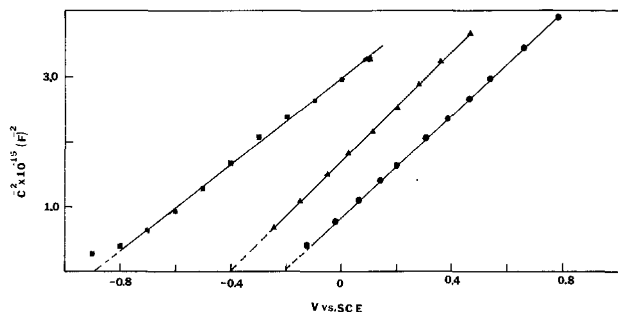

Fig. 5. S-M plot for n-CdS contacting MeCN, 0.1*M* TBAP, containing various redox couples; *f* = 2 kHz blank (■); 10-$MP^{0/+}$ (▲); $Th^{0/+}$ (●) (For abbreviations, see Table II).

probed by conductance measurements (14). If a surface-state level is assumed with a time constant, τ, independent of potential, the measured overall in-phase (0°) component, G_p, of a semiconductor in contact with a liquid electrolyte can be related, under certain conditions (see Appendix), to the surface-state capacitance, C_{ss}, and its time constant (τ) by the following equation (14)

$$\frac{G_p}{\omega} = \frac{G_{ss}}{\omega} + \frac{G_D}{\omega} = \frac{C_{ss}\omega\tau}{1+\omega^2\tau^2} + \frac{G_D}{\omega} \qquad [2]$$

where G_D is the depletion layer conductance, G_{ss} is the surface-state conductance, and ω is the angular frequency. Then a plot of G_p/ω *vs.* ω at a given potential will go through a maximum when $\omega\tau = 1$. The reciprocal of this peak angular frequency will yield a time constant which represents a weighted average of the

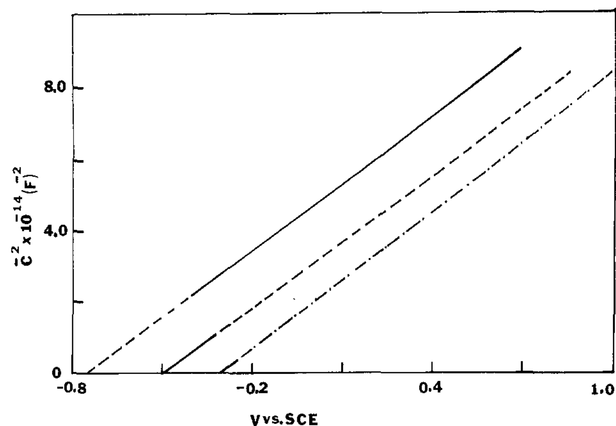

Fig. 6. S-M plots for n-InP/contacting MeCN, 0.1*M* TBAP containing various redox couples *f* = 5 kHz. Blank (——); $MV^{2+/+}$ (---); $Fe(CP)_2^{0/+}$ (—·—·). (For abbreviations, see Table II).

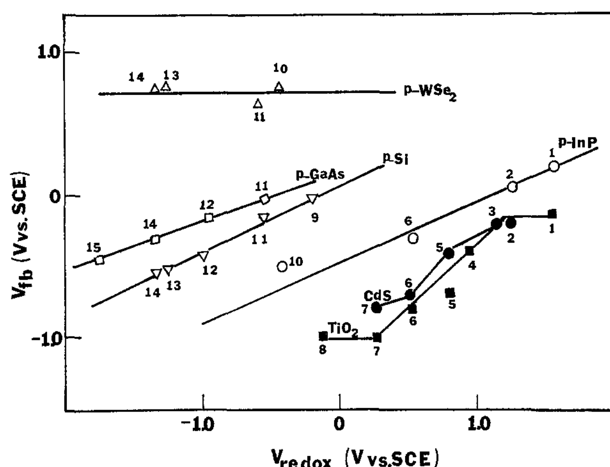

Fig. 7. Plots of variation of V_{FB} with V_{redox} for different semiconductor electrodes in MeCN, 0.1*M* TBAP containing various redox couples. The numbers on the figure represent different redox couples; see Table II.

time constants associated with the surface states located around that potential. For the layer-type compound, n-$MoSe_2$, a plot of G_p/ω *vs.* ω at +0.25V *vs.* SCE, in MeCN, 0.1M TBAP, containing 10-MP is given in Fig. 8a. The time constant, τ, corresponding to the peak frequency evaluated from this plot, is around 1.14×10^{-4} sec. This value of τ is in good agreement with that obtained by Kautek and Gerischer for $MoSe_2$ (26). Notice also that the peaks of the G_p/ω *vs.* ω plots (Fig. 8a) occur at about the same frequency for different applied potentials in the region where the peak is observed in the G_p *vs.* *V* plots; this suggests that τ is relatively independent of potential. With this value of τ, the surface-state density as a function of potential (N_{ss}, in cm^{-2} eV^{-1}) can be calculated from the equation

$$N_{ss} = \frac{2G_{ss}}{e} \cdot \tau \qquad [3]$$

where *e* is the electronic charge. The procedure used to determine G_{ss} is given in the Appendix. A typical plot of N_{ss} (cm^{-2} eV^{-1}) *vs.* *V* is shown for n-$MoSe_2$ over the potential range +0.1-0.45V *vs.* SCE in Fig. 8b. The integrated value of the curve in Fig. 8b when multiplied by τ/e yields the value of N_{ss} (cm^{-2}). Thus for n-$MoSe_2$, the surface-state density in the +0.1-0.45V regime is estimated as about 1.4×10^{10} cm^{-2}. This value of the density of surface states is comparable to that obtained with α-$MoTe_2$ (14) which is 10^{10} cm^{-2}. Similar values for τ and N_{ss} were obtained for n- and p-WSe_2. In Fig. 9a, b are shown the plots of G_p/ω *vs.* ω at −0.1V and N_{ss} *vs.* *V*, respectively, for p-Si.

Downloaded 12 Feb 2009 to 146.6.143.190. Redistribution subject to ECS license or copyright; see http://www.ecsdl.org/terms_use.jsp

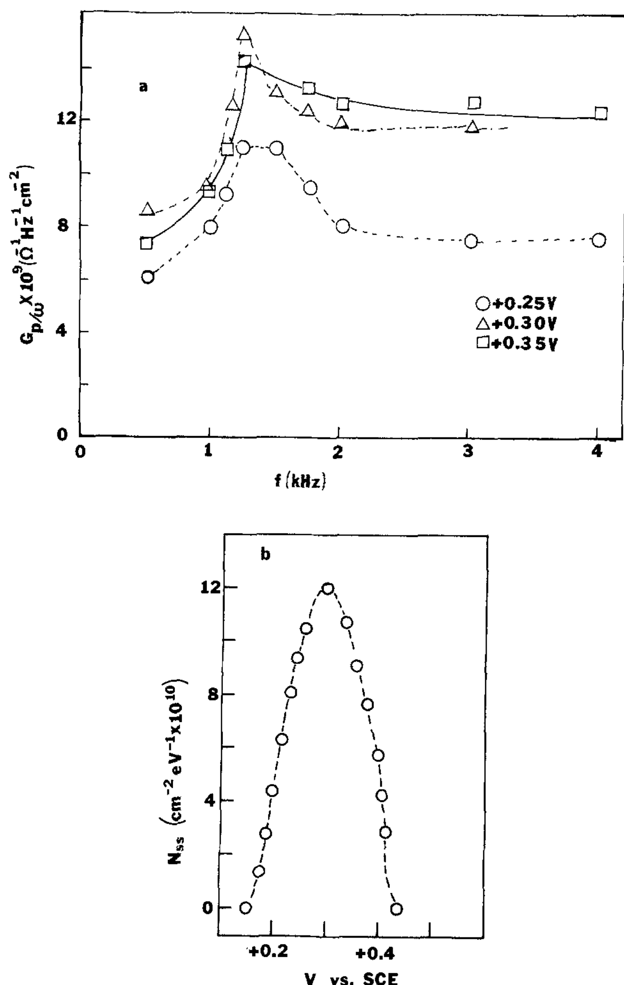

Fig. 8. (a) G_p/ω vs. f (where G_p is the measured equivalent parallel conductance and f is the frequency) for n-$MoSe_2$ in MeCN, 0.1*M* TBAP, 18 m*M* 10-MP at different potentials; (b) N_{SS} vs. V for n-$MoSe_2$ in MeCN, 0.1*M* TBAP containing 18 m*M* 10-MP.

Following the method described above for n-$MoSe_2$, the τ and N_{ss} are about 4×10^{-5} sec and 10^{13} cm^{-2}, respectively.

Effect of pretreatment on TiO_2 behavior.—For TiO_2, the etching procedures documented in literature span a wide regime of chemical activity—from such caustic mixtures as $H_2SO_4/(NH_4)_2SO_4$ (1:1) (27) and molten NaOH (28, 29) to solutions that probably only clean the surface, such as dilute acids (30-32). Molten bisulfates have been shown to dissolve TiO_2 at high temperatures, and $KHSO_4$ as an etchant has been shown to be specific for the TiO_2 (001) face (33). We report below the effects of two different pretreatment procedures (treatment 1 and 2, see Experimental) on the properties of surface states on n-TiO_2 (001). To probe the effects of these two different treatments on the properties of surface states such as time constant, energy, and density distribution, the 0° component was measured both as a function of potential and frequency for two undoped (crystal A) and Nb-doped (crystal B) TiO_2 crystals. In Fig. 10 are shown the G_p *vs.* V curves in MeCN, 0.1*M* TBAP containing 10 m*M* 10-$MP^{0/+}$ for crystal A (treatment 1). For crystal A (treatment 2) such plots are shown in Fig. 11. For Nb-doped TiO_2

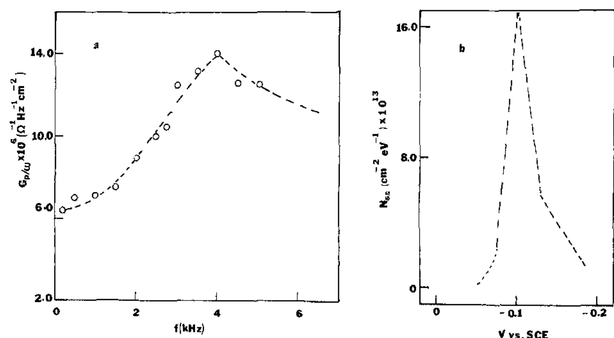

Fig. 9. (a) G_p/ω vs. f for *p*-Si in MeCN, 0.1*M* TBAP at a potential of 0.1V vs. SCE; (b) N_{SS} vs. V for *p*-Si in MeCN, 0.1*M* TBAP.

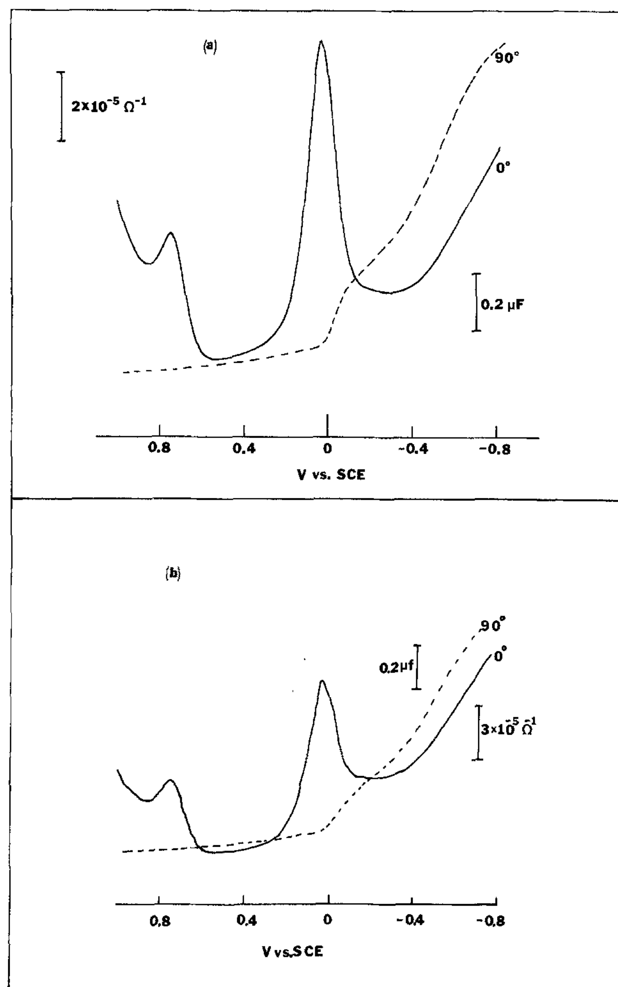

Fig. 10. G_p and C_p vs. V for TiO_2 (crystal A, treatment 1) in MeCN, 0.1*M* TBAP containing 10 m*M* 10-$MP^{0/+}$; (a) $f = 25$ Hz; (b) $f = 50$ Hz.

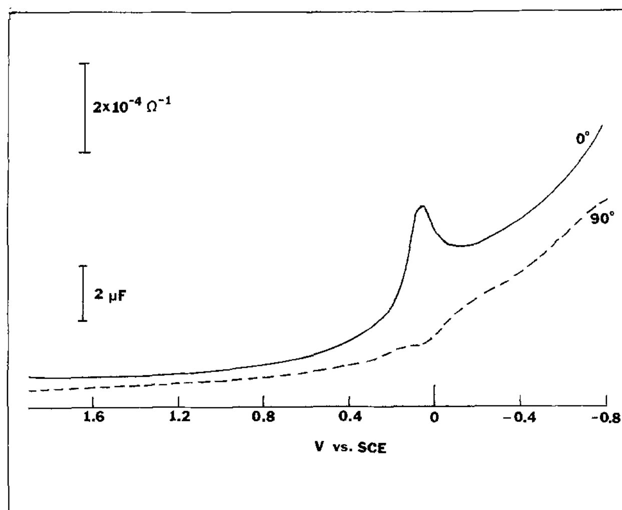

Fig. 11. G_p and C_p vs. V for TiO_2 (crystal A, treatment 2) in MeCN, 0.1*M* TBAP, containing 10 m*M* 10-$MP^{0/+}$; $f = 25$ Hz.

Downloaded 12 Feb 2009 to 146.6.143.190. Redistribution subject to ECS license or copyright; see http://www.ecsdl.org/terms_use.jsp

crystals (treatment 1), G_p *vs.* V plots are given in Fig. 12. The frequencies employed and the concentrations of the redox couples used are given in the respective figure captions. For crystal B, the S-M plots in the presence of different redox couples are shown in Fig. 13. A typical G_p/ω *vs.* ω plot is given for crystal B in Fig. 14. Following the arguments given for n-$MoSe_2$, the time constant, τ, and the density of surface states located around 0V *vs.* SCE are around 8×10^{-5} sec and 10^{10} cm^{-2}, respectively. Similar values of τ and N_{ss} were obtained for crystal A.

Discussion

Not many studies have been reported in literature pertaining to the a-c impedance measurements of semiconductors in nonaqueous solvents (34). Dutoit *et al.* (25) and Tyagai and Kolbasov (35) have made a systematic investigation of the C-V behavior of single crystal TiO_2 and CdS in aqueous solutions. Essentially both of these studies indicate that surface states located within the bandgap influence the mechanism of the overall charge transfer occurring at the interface. For n-TiO_2 (crystal A, treatment 2), the V_{FB} was found to be frequency independent, although there was a marginal variation in the slope (Fig. 3). A similar observation was made by Kabir-ud-Din *et al.* (36), although the V_{FB} values in MeCN reported by them were more negative by about 0.3V than our values; values of V_{FB} closer to ours were reported earlier (8, 37). In the presence of $Fe(\eta^5\text{-}C_5Me_5)_2^{0/+}$ and $TMPD^{0/+}$, which are located above half of the gap, there is little variation in the V_{FB} from the blank solution. However, for couples such as $Fe(Cp)_2^{0/+}$ and 10-$MP^{0/+}$, located below half the gap, the V_{FB} varies monotonically as

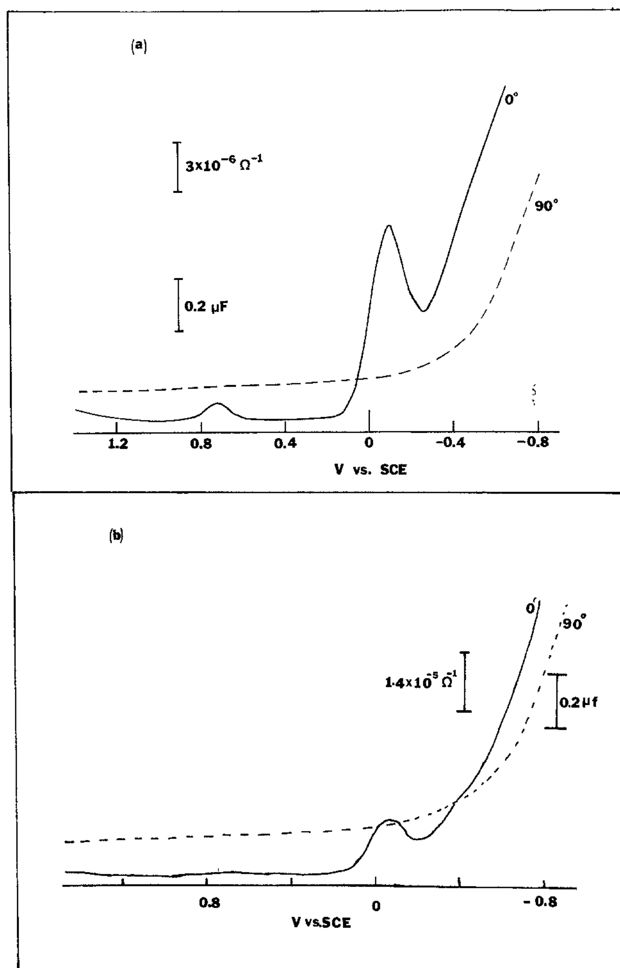

Fig. 12. G_p and C_p *vs.* V for TiO_2 (crystal B) in MeCN, 0.1*M* TBAP containing 10 m*M* 10-$MP^{0/+}$; (a) f = 10 Hz; (b) f = 25 Hz.

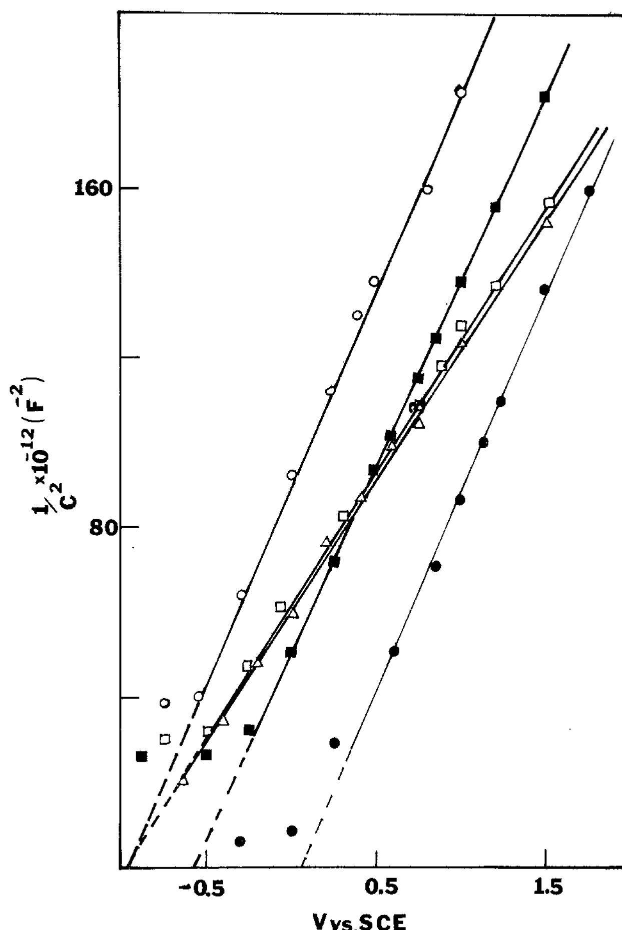

Fig. 13. S-M plots for n-TiO_2 (crystal B) contacting MeCN, 0.1*M* TBAP containing different redox couples; f = 200 Hz; (○) I^-/I_2; (●) $Th^{0/+}$; (△) $[Fe(\eta^5 - C_5Me_5)_2]^{0/+}$; (□) Blank; (■) 10-$MP^{0/+}$.

shown in Fig. 7. In the case of n-CdS, the variation in V_{FB} with V_{redox} is similar to that of n-TiO_2 (see Fig. 7). A similar observation was made by Frese (38) for n-CdSe in aqueous solutions. With p-Si, p-GaAs, and n-InP, the V_{FB} varies montonically with V_{redox} (Fig. 7). In the case of n-InP, the S-M plot is linear for the entire bandgap (Fig. 6); similar observations with n-InP were made by Van Wezemall *et al.* (39) in aqueous solutions and by Tuck *et al.* (40) for solid-state Al/n-InP Schottky barriers. They observed that the S-M plot is linear over a range of 0.8V and deviates slightly thereafter implying the presence of deep donor levels about 0.8V below the conduction band. The layer-type compounds represent a different situation where there is no significant shift in V_{FB} with V_{redox} from that observed in blank solutions for couples with $E^{o\prime}$s located within or outside of the bandgap (Fig. 7). This probably indicates that while for many large and small bandgap semiconductors the role of bandgap surface states is important, for layer-type compounds the surface states have only marginal effects. The time constant associated with surface states on p-Si is around 4×10^{-5} sec, and this falls in the domain of fast surface states. The N_{ss} is around 10^{13} cm^{-2}, and this is high enough for Fermi level pinning to occur.

The surface states on TiO_2 made conductive by reduction are due in part to oxygen vacancies and Ti^{3+}. Several investigators have used different techniques to deduce the presence of these states. These include (*i*) thermal and photoelectronic properties (41), (*ii*) electron spectroscopy (42), (*iii*) catalytic decomposition of N_2O supplemented with EPR studies (43), and (*iv*) low frequency capacitance-voltage method (44). However, in all the methods, the evidence for surface states was not obtained with TiO_2 in contact with an

Downloaded 12 Feb 2009 to 146.6.143.190. Redistribution subject to ECS license or copyright; see http://www.ecsdl.org/terms_use.jsp

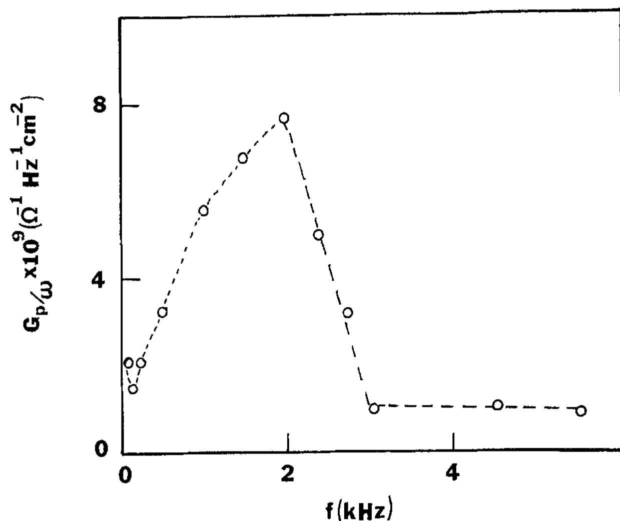

Fig. 14. G_p/ω vs. f for TiO_2 (crystal B) contacting MeCN, 01M TBAP. G_p value was extracted at a potential 0.0V vs. SCE.

electrolyte. Since the properties of the electrode surface dramatically change upon immersion in electrolyte (because of the large electric field in the interfacial region and interaction with solvent and electrolyte), a study of surface states *in situ* produces more meaningful information about the electrode surface. The low frequency *C-V* method, which employs the quadrature component of the a-c impedance, can be employed to study the properties of the surface states, but it suffers from the limitation (15) that the spread in the space charge capacitance values, even when the frequency is increased by one order of magnitude, is only 14%. This means large errors will be introduced in the calculation of the surface-state properties as we discussed in more detail in a recent paper (14). The conductance technique is more useful in extracting surface-state properties. In our studies on the a-c admittance characteristics of n-TiO_2 (crystals A and B, treatment 1), the in-phase component yields evidence for the presence of states at two energies (Fig. 10, 12). However, in the case of TiO_2, crystal A, treatment 2, only one peak in the G_p *vs.* V plot at 0.1V *vs.* SCE is observed (Fig. 11). Based on the evidence obtained by other investigators, we tentatively assign those closer to V_{FB} (shallow level) to oxygen vacancies and those around the middle of the gap (deep levels) to Ti^{3+}, The peak heights are frequency dependent as shown in Fig. 10-12. The shift in V_{FB}'s of the $KHSO_4$-etched TiO_2 crystals to positive values when V_{redox} is below half the gap (Fig. 13) is similar to that observed with crystal A (treatment 2) (see Fig. 7). In all the S-M plots, the deviation from linearity near the V_{FB} is due to the constancy of the capacitance around V_{FB} since at potentials negative of V_{FB} an n-type semiconductor behaves like a metal. For both crystals etched with $KHSO_4$, the peak potentials of the surface states due to Ti^{3+} are located at the same potential (0.72V *vs.* SCE), but those due to oxygen vacancies (shallow levels) are offset by 0.1V (crystal B 0.1V more negative than crystal A). Note that surface states due to Ti^{3+} and oxygen vacancies are present in both the crystals subjected to treatment 1. Thus it appears that in TiO_2 crystals etched with $KHSO_4$, with the reduction by either CO or H_2, two sets of surface states occur. The time constant evaluated from the G_p/ω *vs.* ω plot (Fig. 14) is $\sim 8 \times 10^{-5}$ sec, and the surface-state density for oxygen vacancy is $\sim 10^{10}$ cm^{-2}. This value of N_{ss} is too small for Fermi level pinning to occur (2). The absence of the Ti^{3+} surface-state peak for crystal A, treatment 2 (Fig. 11) is difficult to explain. Perhaps the surface Ti^{3+} ions are oxidized in this crystal or a surface layer forms to block these sites.

Conclusions

Based on the results reported here, we can assign the semiconductors studied here into three categories: (*i*) Small bandgap compound and elemental semiconductors (GaAs, InP, Si) represent a situation where V_{FB} tracks V_{redox} monotonically; (*ii*) Large bandgap semiconductors (TiO_2, CdS) where V_{FB} remains fairly constant for couples located above half of the gap and varies monotonically for couples located below half of the gap; and (*iii*) Layer-type compounds (WSe_2) where V_{FB} does not vary with V_{redox}. Evidence for two sets of surface states on a TiO_2 surface contacting MeCN has been obtained by a-c impedance measurements of the in-phase component of the total admittance. The time constant associated with surface states on TiO_2 surfaces is equal to 8×10^{-5} sec, and the N_{ss} for the level at 0V *vs.* SCE was found to be $\sim 10^{10}$ cm^{-2}. The time constant and the N_{ss} for p-Si are 4×10^{-5} sec and 10^{13} cm^{-2}, respectively. This value of N_{ss} is sufficient for pinning the Fermi level.

Acknowledgment

The support of this work by the Solar Energy Research Institute is gratefully acknowledged. The authors wish to thank Dr. H. S. Jarrett of du Pont and Dr. Y. Nakazumi of Nakazumi Earth Crystals Corporation, Japan, for generously donating the TiO_2 single crystals. We also would like to thank G. Garcia for his help with computer programming.

Manuscript submitted Oct. 25, 1982; revised manuscript received Jan. 21, 1983.

Any discussion of this paper will appear in a Discussion Section to be published in the June 1984 JOURNAL. All discussions for the June 1984 Discussion Section should be submitted by Feb. 1, 1984.

The University of Texas at Austin assisted in meeting the publication costs of this article.

APPENDIX

Figure A-1 is the equivalent circuit of the semiconductor/liquid interface (45), neglecting the contribution from the Helmholtz layer and counterelectrode capacitance as well as the bulk resistance of the semiconductor, resistance of the electrolyte, and the Faradaic impedance. The net equivalent circuit comprises a series combination of surface-state resistance (R_{ss}) and capacitance (C_{ss}) connected in parallel to a parallel combination of space charge layer capacitance (C_D) and resistance (R_D) respectively; these are frequency independent but voltage dependent. The total admittance of the equivalent circuit is $Y_D = G_D + j\omega C_D$ where the in-phase component

$$G_p = \frac{\omega^2 C_{ss}^2 R_{ss}}{1 + R_{ss}^2 \omega^2 C_{ss}^2} + \frac{1}{R_D} \quad \text{[A-1]}$$

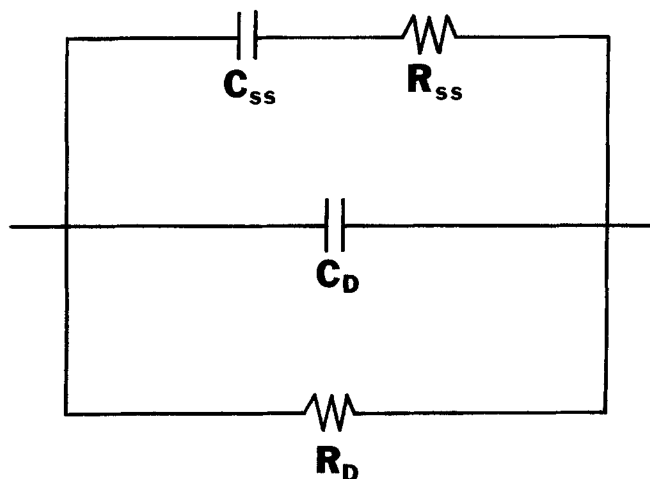

Fig. A-1. Equivalent circuit of the semiconductor/electrolyte interface in the presence of surface states.

Downloaded 12 Feb 2009 to 146.6.143.190. Redistribution subject to ECS license or copyright; see http://www.ecsdl.org/terms_use.jsp

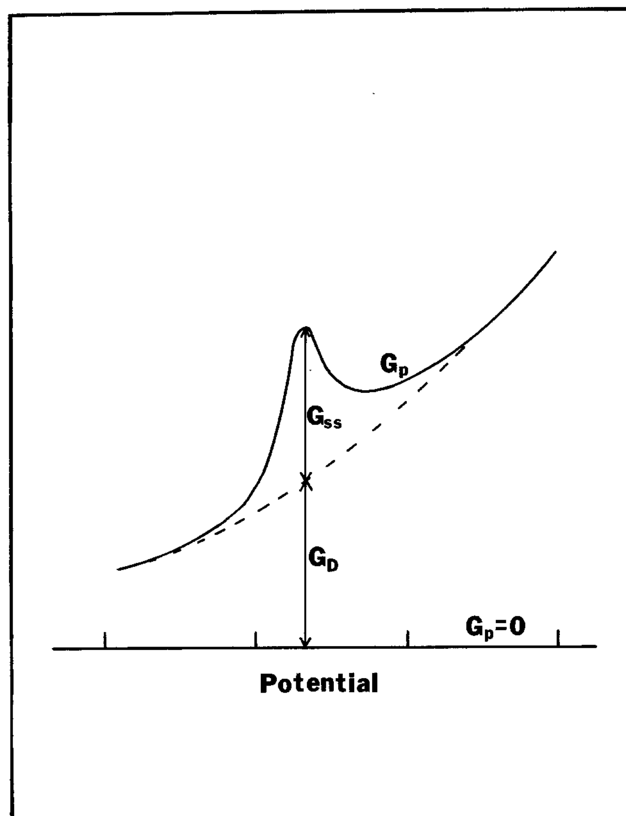

Fig. A-2. Illustration of the method used to extract G_{SS}

and the out-of-phase component

$$C_p = \frac{C_{ss}}{1 + R_{ss}^2 \omega^2 C_{ss}^2} + C_D \quad [A-2]$$

Equations [A-1] and [A-2] can be written as

$$G_p = \frac{\omega^2 \tau C_{ss}}{1 + \omega^2\tau^2} + G_D = G_{ss} + G_D \quad [A-3]$$

and

$$C_p = \frac{C_{ss}}{1 + \omega^2\tau^2} + C_D \quad [A-4]$$

where $G_{ss} = C_{ss}\omega^2\tau/(1 + \omega^2\tau^2)$, $\tau = R_{ss}C_{ss}$, and $G_D = 1/R_D$. G_p can be equated with C_{ss} and hence N_{ss}, only after considering G_D (Eq. [A-3]). Therefore, Eq. [2] holds only when G_D is small compared to G_{ss}. Since G_D (and C_D) are frequency independent, a change in the value of G_D would be manifested in the G_p/ω *vs.* ω plot by a shift parallel to the G_p/ω axis. The ω value corresponding to the peak would not be affected by such a change. Hence, the G_p/ω *vs.* ω plot will always be valid for finding the value of τ independent of the relative values of G_{ss} and G_D.

To determine N_{ss}, Eq. [2] can be written

$$\frac{G_p - G_D}{\omega} = \frac{C_{ss}\omega\tau}{1 + \omega^2\tau^2} \quad [A-5]$$

Theoretically, the G_p/ω *vs.* ω plot should yield values of G_D from the baseline of the plots. However, these plots do not always have flat baselines, and obtaining reliable values of G_D becomes difficult. In these situations, the G_p *vs.* V curves can be more helpful. Values of G_D at a particular potential can be obtained by extrapolating a smooth parabolic baseline in the regime of the peak due to surface states (Fig. A-2). This value can then be subtracted from the measured value of G_p to obtain C_{ss}.

REFERENCES

1. H. Gerischer, in "Physical Chemistry: An Advanced Treatise," Vol. 9A, H. Eyring, D. Henderson, and W. Jost, Editors, p. 463, Academic Press, New York (1970).
2. A. J. Bard, A. B. Bocarsly, F. R. Fan, E. G. Walton, and M. S. Wrighton, *J. Am. Chem. Soc.*, **102**, 3671 (1980).
3. G. Nagasubramanian, B. L. Wheeler, F. R. Fan, and A. J. Bard, *This Journal*, **129**, 1742 (1982).
4. C. A. Mead and W. G. Spitzer, *Phys. Rev.*, **134**, A713 (1964).
5. J. M. Bolts and M. S. Wrighton, *J. Phys. Chem.*, **80**, 2641 (1976); H. Morisaki, M. Hariya, and K. Yazawa, *Appl. Phys. Lett.*, **30** (1977).
6. J. G. Mavroides, V. E. Henrich, H. Zeiger, G. Dresselhaus, J. A. Kafalas, and D. F. Kolesar, in "Electrode Materials and Processes for Energy Conversion and Storage," J. D. E. McIntyre, S. Srinivasan, and F. G. Will, Editors, p. 45, The Electrochemical Society Softbound Proceedings Series, Princeton, NJ (1978).
7. B. Parkinson, F. Decker, J. F. Juliao, M. Abramovich, and H. C. Chagas, *Electrochim. Acta*, **25**, 521 (1980).
8. S. N. Frank and A. J. Bard, *J. Am. Chem. Soc.*, **97**, 7427 (1975); R. N. Noufi, P. A. Kohl, S. N. Frank, and A. J. Bard, *This Journal*, **125**, 246 (1978).
9. E. C. Dutoit, F. Cardon, and W. P. Gomes, *Ber. Bunsenges. Phys. Chem.*, **76**, 81 (1972).
10. J. Vandermolen, W. P. Gomes, and F. Cardon, *This Journal*, **127**, 324 (1980).
11. M. P. Dare-Edwards and A. Hamnett, *J. Electroanal. Chem. Interfacial Electrochem.*, **105**, 283 (1979).
12. J. Gobrecht and H. Gerischer, *Solar Energy Mater.*, **2**, 131 (1979); D. Laser and A. J. Bard, *This Journal*, **123**, 1828 (1976).
13. T. C. McGill, *J. Vac. Sci. Technol.*, **11**, 935 (1974); S. Kurtin, T. C. McGill, and C. A. Mead, *Phys. Rev. Lett.*, **22**, 1433 (1969).
14. G. Nagasubramanian, B. L. Wheeler, G. A. Hope, and A. J. Bard, *This Journal*, **130**, 385 (1983).
15. E. H. Nicollian and A. Goetzberger, *Bell Syst. Tech. J.*, **46**, 1055 (1967).
16. P. R. Barabash and R. S. C. Cobbold, *IEEE Trans. Electron Devices*, **ed-29**, 102 (1982).
17. J. Dubow and K. Rajeshwar, Final Report, Oct. 1981, Submitted to SERI Div., Golden, CO 80401; M. Abe, H. Morisaki, and K. Yazawa, *Jpn. J. Appl. Phys.*, **19**, 1421 (1980).
18. G. Nagasubramanian and A. J. Bard, *This Journal*, **128**, 1055 (1981).
19. H. S. White, F. R. Fan, and A. J. Bard, *ibid.*, **128**, 1045 (1981).
20. F. Di Quarto and A. J. Bard, *J. Electroanal. Chem. Interfacial Electrochem.*, **127**, 43 (1981).
21. P. A. Kohl and A. J. Bard, *This Journal*, **126**, 598 (1979).
22. L. F. Schneemeyer and M. S. Wrighton, *J. Am. Chem. Soc.*, **102**, 6964 (1980).
23. F. R. Fan and A. J. Bard, *This Journal*, **128**, 945 (1981).
24. F. R. Fan and A. J. Bard, *J. Am. Chem. Soc.*, **102**, 3677 (1980).
25. E. C. Dutoit, R. L. Van Meirhaeghe, F. Cardon, and W. P. Gomes, *Ber. Bunsenges. Phys. Chem.*, **79**, 1206 (1975).
26. W. Kautek and H. Gerischer, *Electrochim. Acta*, **27**, 1035 (1982).
27. H. Tamura, H. Yoneyama, C. Iwakura, H. Sakamoto, and S. Murakami, *J. Electroanal. Chem. Interfacial Electrochem.*, **80**, 357 (1977).
28. E. C. Dutoit, F. Cardon, and W. P. Gomes, *Ber. Bunsenges. Phys. Chem.*, **80**, 475 (1976).
29. R. H. Wilson, *J. Appl. Phys.*, **48**, 4292 (1977).
30. T. Ohnishi, Y. Nakato, and H. Tsubomura, *Ber. Bunsenges. Phys. Chem.*, **79**, 523 (1975).
31. M. S. Wrighton, D. S. Ginley, P. T. Wolczanski, A. B. Ellis, D. L. Morse, and A. Linz, *Proc. Natl. Acad. Sci. USA*, **72**, 1518 (1975).
32. D. M. Shub, A. A. Remnev, and V. I. Veselovskii, *Elektrokhimiya*, **9**, 676 (1973).
33. H. S. Jarrett, E. I. du Pont de Nemours and Co., DE, Personal communication.
34. G. Nagasubramanian, B. L. Wheeler, F. R. Fan, and A. J. Bard, in "Photoelectrochemistry: Fundamental Processes and Measurement Techniques," W. L. Wallace, A. J. Nozik, and S. K. Deb, Edi-

Downloaded 12 Feb 2009 to 146.6.143.190. Redistribution subject to ECS license or copyright; see http://www.ecsdl.org/terms_use.jsp

tors p. 372, The Electrochemical Society Softbound Proceedings Series, Vol. 82-3, Pennington, NJ (1982).
35. V. A. Tyagai and G. Ya. Kolbasov, *Surf. Sci.*, **28**, 423 (1971).
36. Kabir-ud-Din, R. C. Owen, and M. A. Fox, *J. Phys. Chem.*, **85**, 1679 (1981).
37. M-S. Lin, N. Hung, and M. S. Wrighton, *J. Electroanal. Chem. Interfacial Electrochem.*, **135**, 121 (1982).
38. K. W. Frese, Jr., *J. Appl. Phys.*, **53**, 1571 (1982).
39. A. M. Van Wezemael, W. H. Laflere, F. Cardon, and W. P. Gomes, *J. Electroanal. Chem. Interfacial Electrochem.*, **87**, 105 (1978).
40. B. Tuck, G. Eftekhari, and D. M. de Cogan, *J. Phys. D: Appl. Phys.*, **15**, 457 (1982).
41. A. K. Ghosh, F. G. Wakim, and R. R. Addiss, Jr., *Phys. Rev.*, **184**, 979 (1969).
42. V. E. Henrich, G. Dresselhaus, and H. J. Zeiger, *Phys. Rev. Lett.*, **36**, 1335 (1976).
43. J. Cunningham and A. L. Penny, *J. Phys. Chem.*, **78**, 870 (1974).
44. K. Kobayashi, Y. Aikawa, and M. Sukigara, *Chem. Lett.*, 679 (1981).
45. W. P. Gomes and F. Cardon, *Ber. Bunsenges. Phys. Chem.*, **74**, 431 (1970).

A Study of the Transition from Oxide Growth to O_2 Evolution at Pt Electrodes in Acid Solutions

V. I. Birss*

Department of Chemistry, University of Ottawa, Ottawa, Ontario, Canada

A. Damjanovic*

Corporate Research and Development, Allied Corporation, Morristown, New Jersey 07960

ABSTRACT

A Pt ring disk electrode was used in acid solutions to study the transition from Pt oxide growth to oxygen evolution and to distinguish the rates of these two processes. When a constant current is applied to the disk electrode, the disk potential, V, initially increases linearly with time, and hence with the charge density, while a negligible current is observed at the ring. In this potential region, essentially all of the applied current is used for the growth of a Pt oxide film. Following the linear V/t region, V continues to increase but now more slowly and nonlinearly with time, while the ring current initially increases sharply and then slowly approaches the value expected for 100% oxygen evolution at the disk electrode. Thus, the Pt oxide film continues to grow in the nonlinear V/t region even when oxygen evolution becomes the major reaction. In the nonlinear V/t region, V again increases nearly linearly with the integrated charge density for oxide film formation or with the oxide film thickness. This V/q relationship in the nonlinear V/t region is different from the V/q relationship in the linear V/t region. However, the mechanism of Pt oxide growth and the properties of the film when the O_2 evolution reaction is the dominant reaction remain the same as in the initial Pt oxide growth region where O_2 evolution is not significant. The distribution of potentials in the oxide film and in the inner and outer Helmholtz layers is discussed.

When a constant anodic current is applied to a prereduced oxide-free Pt electrode starting from the rest potential in O_2-saturated acid or alkaline solutions, $V_R = 0.98V$ *vs.* RHE (1), three distinct potential regions can be seen in a V/t transient (2-5). Initially, the potential increases rapidly and nonlinearly with time as the first monolayer of an oxide film is formed (5-7). Following this region, the electrode potential increases fairly linearly with time (Fig. 1) with the current being used for further growth of the oxide film (8). Eventually at higher potentials, oxygen evolution begins and soon becomes the major electrode reaction.

In Fig. 1, potential/time curves are shown for three constant current densities in a $0.2N$ H_2SO_4 solution. In this figure, the time axis has been scaled for each current density to represent charge density, $q = it$. At a particular potential, which depends on the applied current density and the pH, the linear increase of the potential with time, or charge density, ceases. Now, the potential increases at a rate which decreases with time while O_2 evolution continues to increase and soon becomes the predominant electrode reaction (9). Previous work has shown that at long times the potential changes nearly linearly with the logarithm of time of polarization and the oxide film continues to grow at a very slow rate (3, 9, 10).

In this study, a Pt ring disk electrode has been used to separate the reactions of Pt oxide growth and O_2 evolution. A comparative analysis of their individual rates and their dependence on the electrode potential is expected to yield information on the nature of the changes in the kinetics of oxide growth and on the potential distribution across the complex interface, comprised of the oxide film and the inner and outer Helmholtz layers, during the transition from the oxide growth to O_2 evolution. Such an analysis is also expected to aid in the overall understanding of the mechanism of the O_2 evolution reaction at oxide-covered electrodes.

* Electrochemical Society Active Member.
Key words: metal, kinetics, chemisorption.

Experimental

A commercially designed Pt disk-Pt ring electrode (Pine Instrument Company, disk radius 0.383 cm, ring inner radius 0.399 cm, and ring outside radius 0.422 cm) was utilized in an all-glass cell similar to that described in (11). The ring-disk electrode was polished to a mirror finish with alumina paste. In some experiments, a thin layer of gold (~1000Å) was electrodeposited over the ring electrode. A saturated calomel electrode in a separate compartment served as the reference electrode, and a Luggin capillary extended upwards toward the center of the disk electrode. A Pt counterelectrode was placed in the same compartment as the ring disk electrode.

Solutions were prepared from reagent grade sulfuric acid and conductivity water. No extensive purification of solutions was carried out, *e.g.*, by preelectrolysis. In all experiments, solutions were first purged of O_2 with high purity Ar. During electrochemical measurements, Ar was passed over the solution.

Prior to each series of experiments, the disk electrode was anodically oxidized and cathodically re-

Downloaded 12 Feb 2009 to 146.6.143.190. Redistribution subject to ECS license or copyright; see http://www.ecsdl.org/terms_use.jsp